Investigation of laser-induced inter-welding between Au and Ag nanoparticles and the plasmonic properties of welded dimers

Journal:	*Nanoscale*
Manuscript ID	NR-ART-09-2018-007718.R1
Article Type:	Paper
Date Submitted by the Author:	06-Nov-2018
Complete List of Authors:	Xu, Xiaohui; Purdue University, Materials Engineering Isik, Tugba; Purdue University, Mechanical Engineering Kundu, Subhajit; Purdue University, Materials Engineering Ortalan, Volkan; University of Connecticut, Materials Science and Engineering

SCHOLARONE™
Manuscripts

Nanoscale

ARTICLE

Investigation of laser-induced inter-welding between Au and Ag nanoparticles and the plasmonic properties of welded dimers

Xiaohui Xu,[c] Tugba Isik,[b,d] Subhajit Kundu,[c] and Volkan Ortalan[a,b,*]

Noble metallic nanoparticles with unique plasmonic properties are useful in a variety of applications including bio-imaging, sensing, cancer therapy, etc. The properties of metallic nanoparticles can be tuned by multiple ways, among which laser welding is a highly efficient method. In this study, laser-induced inter-welding of Ag-Au nanoparticle (NP) dimers was investigated using *in situ* transmission electron microscopy (TEM) and energy-dispersive X-ray spectroscopy (EDX). For the first time, the welding process was directly visualized. The structural and compositional evolution of Ag-Au dimers were studied in detail, and several typical nanostructures formed during the welding process, including two types of core-shell structures, were discovered. Based on these observations, we proposed a complete mechanism explaining how welding proceeds under the influence of laser. Finite difference time domain (FDTD) simulations demonstrated that the plasmonic properties of welded Ag-Au dimers were different from those of pure Au-Au or Ag-Ag dimers and can be tuned by forming shells, alloying or changing the size ratio of Ag and Au NPs.

Introduction

Noble metallic nanoparticles (NPs), such as gold and silver, have been extensively studied in the past few decades due to their wide applications in biosensing, [1] imaging, [2] cancer therapy, [3] nanophotonics, [4] etc. Those applications are closely related to the unique optical and plasmonic properties of metallic NPs originating from the collective oscillations of conduction electrons under an external electromagnetic radiation, known as localized surface plasmon resonance (LSPR). It has been well established that the LSPR behavior of gold or silver NPs has a strong dependence on the morphology of nanoparticles, including size, shape, composition, etc., [5–7] which has facilitated the development of multiple synthetic routes to obtain NPs with various sizes and shapes for specific uses. [8–12] The optical and plasmonic properties of metallic NPs can also be modified after synthesis by welding or sintering, which has attracted much interest in recent years. [13,14] Metallic NPs can be sintered or welded together optically, thermally or spontaneously by cold welding. [13,15–17] Laser welding, as a special kind of light-induced welding, has been widely used for welding nanostructures such as nanowires and nanoparticles.

[17–19] Due to the 'hot spot' effect [20] between adjacent plasmonic NPs under a laser with specific wavelength, NPs can be preferentially heated at the interparticle gap, resulting in a higher welding efficiency compared with the uniform thermal welding.

Despite the progress in the study of nanoparticle welding, *in situ* investigations of welding in nanoparticles with different compositions have been very scarce. For instance, although the welding of gold or silver NPs have been investigated in numerous studies, [14,17,21–23], most of them are focused on the welding between NPs with the same composition, i.e. Ag-Ag or Au-Au welding. Study on the welding between gold and silver NPs (Ag-Au welding) is very limited. [24] However, based on the differences in optical, plasmonic and chemical properties between gold and silver NPs, [8,25,26] Ag-Au welding might provide a novel way to combine their various features and obtain functional nano-blocks with unique properties. Moreover, *in situ* study of the welding process, especially laser-induced welding, is extremely rare due to the difficulty in conducting laser experiments inside an electron microscope system. This has prevented researchers from gaining a better understanding towards laser-induced welding of NPs since a complete picture of the structural and compositional evolution is missing. Fortunately, the advent and development of ultrafast transmission electron microscopy (UTEM) makes *in situ* nanoscale investigation of laser-induced dynamical processes possible. [27–31] The direct visualization enabled by UTEM helps to reveal more details about the structural evolution of Au-Ag welding leading to a more mechanistic understanding for this process.

In this paper, the welding/sintering between gold and silver NPs supported on TEM grids induced by nanosecond pulsed

[a.] *Materials Science and Engineering, University of Connecticut, Storrs, Connecticut 06269, United States.*

[b.] *Institute of Materials Science, University of Connecticut, Storrs, Connecticut 06269, United States.*

[c.] *School of Materials Engineering, Purdue University, 701 West Stadium Avenue, West Lafayette, Indiana, 47907, United States.*

[d.] *School of Mechanical Engineering, Purdue University, 585 Purdue Mall, West Lafayette, Indiana, 47907, United States.*

[*] Email: vortalan@uconn.edu.

[†] Electronic Supplementary Information (ESI) available: See DOI: 10.1039/x0xx00000x

laser was studied. For the first time, UTEM was utilized to investigate the welding process in real time. Aiming at understanding the welding process and involved mechanisms, we focused on two-nanoparticle welding as it is the most fundamental case and the key to understanding the welding of more complicated structures. Both the structural and compositional evolutions of the Au-Ag NP pairs were examined using UTEM, scanning transmission electron microscopy (STEM) and energy-dispersive X-ray spectroscopy (EDX). Results showed that the inter-welding of Au and Ag NPs starts with the formation of a neck between two particles, then a silver shell around the Au NP, followed by an Au shell around the Ag NP, and finally the formation of two Au/Ag alloy NPs. To the best of our knowledge, this is the first systematic study of the welding of Ag-Au heterodimers. We also examined the optical properties of the dimers formed after welding using finite difference time domain (FDTD) method and showed that inter-welding of Ag and Au NPs results in dimers with unique LSPR spectra compared to pure Ag-Ag and Au-Au dimers. This might inspire the design of nanoparticle-based plasmonic devices with flexible optical responses.

Experimental

TEM experiments and characterization

Ag colloid purchased from Sigma Aldrich (60 nm particle size, 0.02 mg/mL in aqueous buffer, product #730815) and Au colloid purchased from Nanopartz (50 nm particle size, 50 µg/mL, 18MEG DI water buffer, product #A11-50-CIT-DIH-25) were mixed with 1:1 ratio and then dispersed onto a carbon-coated copper grid. *In situ* laser experiments were performed inside an ultrafast transmission electron microscope (UTEM) based on an FEI Tecnai G20 system. A frequency doubled Nd-YAG pulsed laser beam with a wavelength of 532 nm, pulse width of 1 ns, frequency of 25 kHz and $1/e^2$ spot size of ~80 µm was used as sample excitation laser. Laser power ranging from

0.4 mW to 3 mW were used in different experiments. An external delay generator was used to set laser in duty cycle mode, and different numbers of on-pulses and off-pulses in one cycle were tested and used to get images and videos.

NPs after laser irradiation were characterized by high angle annular dark-field scanning transmission electron microscopy (HAADF-STEM) imaging and energy-dispersive X-ray spectroscopy (EDX) using FEI Titan EFTEM 80-300 kV.

FDTD simulation

The FDTD simulation was performed using the free software MEEP. [32] The absorption efficiency of four types of dimers, i.e. Ag-Ag dimer, Au-Au dimer, Ag-Au dimer and Ag-Au@Ag core-shell dimer, have been simulated and compared. All of them are composed of two NPs with an overlapping distance of 4nm to show welding. To study the effect of composition, dimers were simulated with the same geometry, i.e. a 60nm-sized NP plus a 50nm-sized NP. Specifically, in the Ag-Au@Ag dimer, the Ag shell thickness is set to be 2nm estimated from experimental observation, thus the diameter of the Au NP inside is set to be 46nm. The electric field distribution around the Ag-Au dimer and Ag-Au@Ag dimer were also simulated to demonstrate the local field enhancement. To study the effect of Ag-Au NP size ratio, the absorption efficiency of a dimer with both equally sized Au and Ag NPs (50nm) was calculated and compared with the previous Ag-Au dimer. A Gaussian electromagnetic source with a central frequency of 660 THz and a frequency span of 720 THz was used and the electric field was polarized along the longitudinal direction of dimers.

Results and discussion

Figure 1a shows the schematic of UTEM utilized to study the laser welding of Ag-Au NP dimers. A sample excitation laser controlled by an electronic delay generator is used to initiate structural changes in the sample. Ag colloid with an average
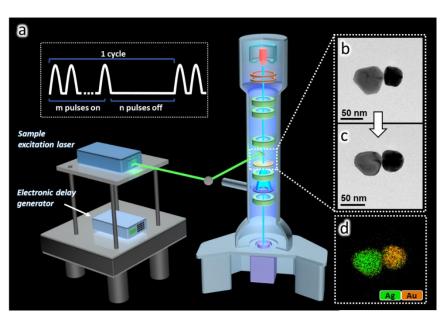

Figure 1. (a) Schematic of UTEM used for the in situ laser irradiation experiment. Inset: profile of the sample excitation laser in duty cycle mode. (b) and (c) are TEM images showing an Au-Ag NP dimer (b) before and (c) after laser irradiation. (d) shows the EDX mapping of the same dimer after laser irradiation.

particle size of 60 nm and Au colloid with an average size of 50 nm were mixed and then dispersed onto a TEM grid for *in situ* laser experiments. We chose slightly different sizes for the two species in order to distinguish Ag-Au NP dimers from pure Ag-Ag and Au-Au dimers. Both gold and silver NPs used in this study have a characteristic five-fold twined structure. [33–35] Considering the variation of NP concentration and laser alignment in different experiments, laser power ranging from 1 mW to 3 mW has been used. In order to observe the details of the nanoparticle welding by slowing down the dynamic processes, a duty cycle mode was adopted, in which some off-pulses are put between trains of on-pulses (see Figure 1 inset). Figure 1b and 1c show the bright field TEM images of two NPs before and after laser irradiation. EDX mapping from the same region was also obtained after laser as shown in Figure 1d. The Ag NP is highly faceted before laser exposure but becomes more rounded after laser treatment. Besides, both NPs display noticeable size changes during the experiment, as Ag NP shrinks while Au NP becomes larger. This might be an indication of inter-diffusion between Ag NP and Au NP, which can also be seen in Figure 1d. Although the structural evolution of metallic NPs during welding has been studied extensively, [17,36–38] few studies have reported the compositional evolution of NPs with different atomic species. Therefore, we investigated both the structural and compositional changes of Ag-Au NP dimers during welding in our experiments.

The structural evolution of a typical Ag-Au NP pair under laser irradiation with time was recorded with both videos (see supplementary information) and images taken after different number of laser pulses. NP dimers exposed to only electron beam were also monitored (Figure S1) to determine the influence of the electron beam on welding. The results confirmed that the electron beam itself has negligible impact on the welding or structural change of the nanoparticles

different atomic species, i.e. Au and Ag, we carried out high angle annular dark-field scanning transmission electron microscopy (HAADF-STEM) imaging [39] after laser experiments. Au shows a higher contrast in HAADF-STEM images than Ag since elements with higher atomic numbers cause more electrons to be scattered to higher angles. [40,41] Figure 2 shows a series of images take from the same NPs exposed to increasing number of laser pulses. It is observed that with increasing laser irradiation time, a neck forms between two NPs and extends, indicating a localized heating at the inter-particle gap due to the highly localized electromagnetic field at the gap, also referred to as the second generation of hotspots. [42] With heat preferentially generated at the gap, a neck forms and grows by surface diffusion to reduce the large curvature and total surface area. [43] Theoretically, two NPs should completely merge into one to achieve a minimized surface free energy, [44] which, however, is not observed in our experiment. This partial coalescence may be explained by two reasons. Firstly, we used rather low laser powers as a way to slow down the transformation and observe more details. Therefore, the rate of particle coalescence is greatly suppressed. Although there is also heat released from the coalescing boundary due to the reduction of surface energy, [45] it is almost negligible considering the heat loss due to conduction of heat to the whole mass of two NPs with diameters around 50 nm. [43,44] Secondly, with decreasing total surface area, the driving force for coalescence also decreases, leading to slower and slower welding or coalescence process. This is confirmed by the decreasing rate of neck growth with time in Figure 2. As a result, a complete coalescence can only be achieved after a sufficiently long time which is not the focus of our study.

The compositional evolution of Ag-Au NPs was studied by both HAADF-STEM images and EDX mapping, as shown in Figure 3. EDX analysis reveals four types of composition configurations after laser experiments: in Figure 3a, an Au NP and an Ag NP
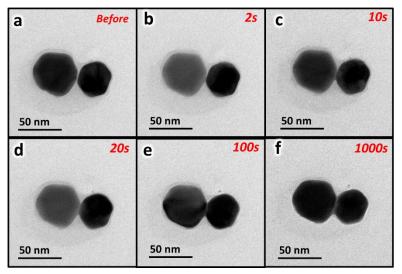

Figure 2. Bright field TEM images of a NP dimer before laser exposure (a) and after being exposed to pulsed laser for 2s (b), 10s (c), 20s (d), 100s (e) and 1000s (f). A duty cycle mode was used with 10 laser pulses on and 90 pulses off in each cycle. Laser power was 0.4mW.

compared with laser. To differentiate nanoparticles with are connected by a small neck without notable inter-diffusion
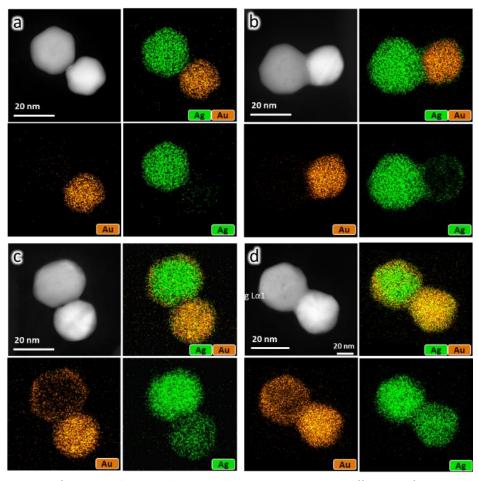
Figure 3. HAADF-STEM images of Ag-Au NP dimers and corresponding EDX mapping. Four different configurations have been probed: (a) The Ag and Au NPs are welded together without visible inter-diffusion; (b) A silver shell is formed over the Au NP; (c) a gold shell is formed over the Ag NP, while the other NP forms an alloy; (d) the Au shell is mixing with the Ag NP inside, leading to a dimer with two alloy NPs. All EDX mappings have been processed by Gaussian blurring fur better view.

between them. In Figure 3b, the Au NP is covered by a thin silver shell, giving an Au@Ag core-shell structure. In Figure 3c, an Au shell is formed around Ag NP, connected with an alloy NP. In Figure 3d, more gold atoms diffuse into the Ag NP and the Au shell formed in Figure 3c has started to diffuse and mix with the Ag NP inside, indicating an alloying process. To show the core-shell and alloy structures more clearly, EDX line-scan were also performed for dimers in Figure 3b-3d (see Figure S2). We believe this is the first time that two kinds of Ag-Au core-shell structures are probed before the formation of Au-Ag alloy in the welding of Au-Ag NP dimers.

Ag-Au bimetallic NPs, including alloy and core-shell structures, have been widely studied in the past few decades and various preparation methods have been developed. [46–50] However, most synthesis methods reported are based on chemical or radiolytic reduction of metallic ions in aqueous medium or organic solvents. [46–49] Laser has also been utilized to investigate Ag-Au bimetallic NPs as reported by a few studies. [24,26,50] For example, Ag@Au core-shell NPs can be synthesized using pulsed laser to ablate Au target in Ag NP colloid, [26] and Ag/Au alloy can be formed by laser-induced inter-diffusion in

Ag-Au core-shell NPs. [50] In a specific study, [24] Peng et al studied the laser irradiation of a mixture of Ag and Au NPs. However, unlike in this study, only the formation of Ag/Au alloy was reported. The missing of core-shell structures in their experiments may be due to the high laser power or long laser irradiation time.

Based on the distinct structures observed, we divide the welding of Au-Ag NPs into five stages (Figure 4): i) Neck formation, ii) Ag-shell formation, iii) Au-shell formation, iv) alloy dimer formation and v) homogeneous alloy NP formation. In the following paragraphs, all five stages will be discussed in detail including possible mechanisms involved.

The neck formation, as discussed previously, is induced by the localized heating at the inter-particle gap. This preferential heating does not end after two NPs are welded together, instead, it moves along the seam formed by the welding and results in the growth of neck. [51] During this process, surface diffusion plays a key role in transporting materials to the neck region, with laser pulses providing essential energy to overcome the diffusion barrier. Soon after this, an Ag shell is formed around the Au NP, which can be explained from
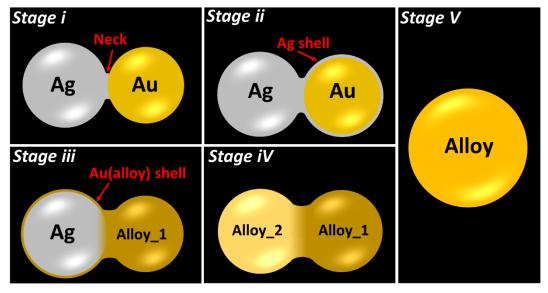
Figure 4. Schematic of the welding process of Au-Ag NPs (cross-sectional view). Stage i: Formation of neck; Stage ii: formation of a silver shell over the Au NP; Stage iii: formation of a gold shell over the Ag NP and a Ag/Au alloy NP; Stage iv: formation of two alloy NPs. Those two alloy NPs are expected to merge into one homogeneous NP after a sufficiently long time, as shown in Stage v.

different perspectives. On one hand, since surface diffusion is driven by the reduction of surface free energy, an Ag shell formed around Au NP must have reduced the total free energy of the NP system. Experimental values of the surface energy of Ag and Au crystals [52,53] are 1.25 J/m^2 and 1.50 J/m^2, respectively, which implies that enclosing Au NP with a thin Ag shell does reduce the total surface free energy. On the other hand, this surface diffusion can be regarded as a wetting process. It has been reported that [54] an Ag NP would wet an Au NP on contact and wrap it in a pulling up-like process, while Au remains almost unchanged. This is because Ag has better structural adaptability compared with Au. In other words, Ag is "softer" than Au and can spread onto Au surface like a liquidlike material. Due to the "softness" feature, Ag NPs can wrap Au NPs up no matter which particle is larger, as illustrated in Figure 5a and 5b, which cannot be explained by the well-established Ostwald ripening theory. This phenomenon is even more evident in the multi-particle welding system shown in Figure 5c: Two Au NPs are wrapped up together by an Ag shell originating from the Ag NP atop

them. Furthermore, the Au NPs inside the Ag shell maintain well-defined boundaries, demonstrating their "solid" nature compared with "soft" Ag. [54] In some regions, the reshaping of Ag and Au NPs from faceted crystals to particles with spherical-like shapes was observed (Figure 1c and Figure S3), indicating a surface melting process. It has been found that surface melting of noble metallic NPs, especially for Ag, occurs at temperatures much lower than their bulk melting points. [55,56] Therefore, it is reasonable to infer that both NPs have formed liquids on their surface after absorbing the photon energy provided by the laser. Considering the surface tension of molten Ag (~0.89 N*m^{-2}) and Au (~1.13 N*m^{-2}),[54] it is still favorable to have Ag "wet" the surface of Au.

In stage iii, the Au@Ag core-shell structure formed in stage ii became Ag/Au alloy, whereas the pure Ag NP on the other side is surrounded by an Au layer (Figure 3c and Figure 4). It is not surprising to see the alloying of Au@Ag core-shell structure, which has been observed in previous studies. [57–59] Two main mechanisms have been reported for this alloying process: one is surface melting [57] and the other is the presence of vacancies
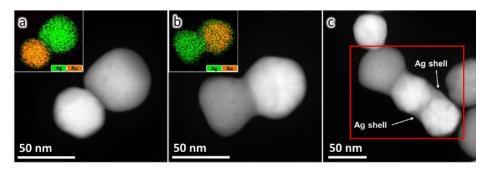

Figure 5. HAADF-STEM images and EDX mapping showing Ag wrapping up Au NPs when (a) Ag NP is larger than Au NP and (b) Ag NP is smaller than Au NP. In (c), the Ag NP in the red square wraps up two Au NPs, while the wrapped Au NPs still remain clear boundaries, indicating the "solid" nature of Au compared with Ag.
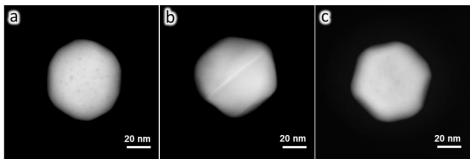
Figure 6. HAADF-STEM images of (a) an Ag NP after laser irradiation, (b) an Au NP after laser irradiation and (c) an Ag NP only exposed to electron beam.

or lattice defects at the core-shell interface. [58] We believe that both mechanisms are involved here. As mentioned before, surface melting is observed in our experiments. Provided that the liquid layer is thicker than the initial Ag shell, [57] the inter-diffusion between Au and Ag at the core-shell interface will be dramatically accelerated due to the high diffusivity of liquid metals. On the other hand, it has been demonstrated that there are vacancies residing at the bimetallic interface which are believed to facilitate the alloying process by vacancy migration.[58] Although the spontaneous alloying of Au@Ag core-shell NP at room temperature is rather slow (takes weeks[58]), it can be remarkably accelerated if an external energy source, such as laser, is provided. Furthermore, laser ablation and/or electron beam create additional voids/vacancies on Ag NP surface as shown in Figure 6, which greatly increase the probability of vacancies migrating to the core-shell interface to enhance alloying.

The formation of Ag@Au core-shell (Figure 3c), to our knowledge, is the first time that Au is observed to form a shell around Ag without using any chemical reduction or surface deposition method. [60,61] This can also be an Au/Ag alloy shell considering that the Au NP has formed an alloy with the Ag shell in the same stage. However, here, we will simply regard it as an Au shell to indicate the flow of Au atoms towards the Ag NP. the Formation of the Au shell is an important sign of the inter-diffusion between two NPs, which can be explained from an energy minimization perspective. It has been reported that forming an Ag-Au bond by breaking Au-Au and Ag-Ag bonds leads to an energy gain of 0.36eV per pair.[54] Therefore, forming Au/Au alloy is energetically favorable. However, there is a kinetic barrier for the alloying to happen, and that is why the Ag@Au or Au@Ag core-shell structures are stable under specific conditions. In our experiments, pulsed laser provides essential energy to overcome the barrier which accelerates the diffusion of Au towards the Ag NP in preparation for the alloying process. Au atoms prefer to diffuse along the surface of Ag NPs because Ag atoms on surface are more energetic than those in the interior thus more diffusive with Au atoms nearby.[54] Besides, a notable number of pores/voids are observed on Ag NP surface after laser experiments as shown in Figure 6a, whereas such pores/voids are not present on Au NPs (Figure 6b). To determine if such defects are caused purely by laser or by both laser and the electron beam, we also

collected STEM images of an Ag NP which has only been exposed to the electron beam. It shows that pure electron beam alone can create some minor pores on the Ag NP (Figure 6c). Therefore, we conclude that Ag is much more sensitive to laser and electron beam than Au. Since voids/pores generate defective lattice sites that are more active than perfect lattice positions, they also help to enhance the surface diffusion of Au atoms via vacancy diffusion. In stage iv, the Ag@Au core-shell structure described above transforms into an Ag-rich alloy (Figure 3d&4). We believe this alloying process are related to the defects at the core-shell interface as well as the energy provided by laser. At the end of this stage, both NPs have transformed into uniform alloys, except that one is rich in Au while the other is rich in Ag. In principle, those two NPs will merge or coalesce into a homogeneous NP since Au and Ag are completely intermiscible and the system needs to minimize the total surface area. This is denoted as the final stage or stage v (Figure 4). However, it takes a long time to achieve this stage based on the low laser power and the decreasing driving force as more surface area is consumed.

The plasmonic property of the nanostructures formed in stage i and ii (denoted as Ag-Au dimer and Ag-Au@Ag dimer respectively) were investigated using three-dimensional (3D) finite difference time domain (FDTD) method and compared to that of pure Ag and Au NP dimers. Analogous to the discussion in a previous work,[62] we can also refer to the Ag-Au dimer as a bimetallic dimer since Ag and Au are separated side by side in the dimer, and refer to the Ag-Au@Ag dimer as a core-shell dimer. This new denotation will be used in the remainder of the discussion. Since the extinction of Ag or Au NPs with diameters around 50~60nm is dominated by absorption, we focused on the absorption efficiencies of dimers. All dimers used in the simulation shown in Figure 7a have the same geometry to eliminate the effect of size difference (see Figure 7a inset). For the core-shell dimer, the Ag shell thickness is set to be 2nm based on experimental observation. In Figure 7a, it is clear that all the four structures have a dominant peak in the near-infrared region, corresponding to the long-wavelength dipolar mode. [14,63] Other mild peaks in the wavelength range 350nm~600nm are related to short-wavelength, higher-order resonance modes. Compared to single Ag and Au NPs, the dipolar resonance peaks of welded dimers have red-shifted significantly, which agrees with previous reports [14,63] and is
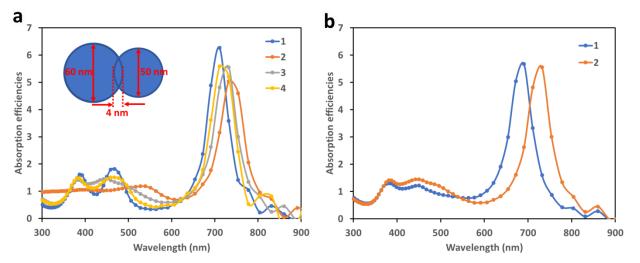
Figure 7. (a) Absorption efficiencies of four types of dimers: 1. Ag NP (60nm) + Ag NP (50nm), 2. Au NP (60nm) + Au NP (50nm), 3. Ag NP (60nm) + Au NP (50nm), 4. Ag NP (60nm) + Au@Ag core-shell NP with a core size of 46nm and shell thickness of 2nm. The overall geometry of those four dimers are set to be the same, i.e. two spherical NPs with dimeters of 60nm and 50nm and an overlapping distance of 4nm. (b) Comparison of the absorption efficiencies of Ag-Au NP dimers with different Ag NP sizes but the same Au NP size. Curve 1: Ag NP (50nm) + Au NP (50nm) with a 4nm overlapping; curve 2: Ag NP (60nm) + Au NP (50nm) with a 4nm overlapping.

explained by charge transfer plasmon. [64] This redshift provides nanostructures with LSPR spectra different from that of single Ag or Au NPs. Besides, the bimetallic dimer and core-shell dimer have their dipolar resonance peaks between that of Ag-Ag and Au-Au dimers, which is reasonable since we are combining Au and Ag in one dimer. The electric field around the bimetallic dimer and core-shell dimer at plasmon resonance were also simulated and shown in Figure S4. It is not surprising to see remarkable field enhancement at the neck region, [14] which provides a promising structure for surface-enhanced Raman scattering (SERS) spectroscopy. Furthermore, we examined the effect of NP size ratio as we are using asymmetric NP dimers in our experiments, and it was found that changing the relative size of Au and Ag NP also changes the LSPR behavior of the dimer they formed (Figure 7b). Therefore, we conclude that the inter-welding of Ag and Au NPs provides dimers with LSPR behaviors that are different from their pure dimer counterparts and can be further tuned by changing the size ratio of Ag and Au NPs.

Structures formed in stage iii, iv and v were not simulated considering the complexity of simulating Au-Ag alloy NPs with varying composition. However, based on previous studies, [46,65] the resonance peak of Au-Ag alloy NP will lie between that of pure Ag and pure Au, varying with the fraction of Ag. This provides another way to tune the optical response of Ag-Au NP dimers.

Conclusions

In this paper, nanosecond pulsed laser-induced welding between Ag and Au NPs was investigated. *In situ* laser experiments were performed inside an ultrafast transmission electron microscope using the sample excitation laser. Direct

visualization of the welding process by videos and images showed that Au and Ag NPs were welded together by neck formation due to the large curvature difference and the "hotspot" effect at interparticle gaps. The size of neck grew with time to reduce the total surface area of the two NPs. Composition of the Ag-Au bimetallic NPs was studied by EDX and HAADF-STEM imaging. It was revealed that four distinct structures were formed in the welding process, namely, Ag-Au dimer, Ag-Au@Ag dimer, Ag@Au-Ag/Au dimer and Ag/Au alloy dimer. Based on this, a complete mechanism describing the structural and compositional evolution of Au-Ag dimers during welding was proposed. Furthermore, FDTD simulation reveals that the optical response of welded Ag-Au dimers is different from that of pure Ag or Au dimers and can be tuned by forming core-shell structures or changing the size ratio of Ag and Au NPs. In conclusion, we believe what we found in this paper provides new strategies to fabricate novel plasmonic devices with unique LSPR properties based on Au-Ag heterodimers. At the same time, UTEM has proved to be a powerful tool for the systematic study of laser-induced material transformations. With the easy control of laser parameters and direct visualization of dynamic processes at nano-scale, UTEM is going to play a key role in the field of *in situ* electron microscopy and laser-matter interaction studies.

Conflicts of interest

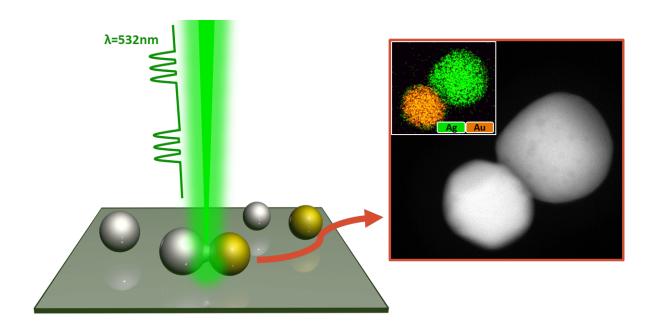The authors state no potential conflict of interest.

References

1   J. N. Anker, W. P. Hall, O. Lyandres, N. C. Shah, J. Zhao and R. P. Van Duyne, *Nat. Mater.*, 2008, **7**, 442–453.

2   K. Sokolov, M. Follen, J. Aaron, I. Pavlova, A. Malpica, R. Lotan and R. Richards-Kortum, *Cancer Res.*, 2003, **63**, 1999–2004.

3   I. H. El-Sayed, X. Huang and M. A. El-Sayed, *Cancer Lett.*, 2006, **239**, 129–135.

4   E. Ozbay, *Science (80-.).*, 2006, **311**, 189–193.

5   K. L. Kelly, E. Coronado, L. L. Zhao and G. C. Schatz, *J. Phys. Chem. B*, 2003, **107**, 668–677.

6   J. B. Jackson and N. J. Halas, *J. Phys. Chem. B*, 2001, **105**, 2743–2746.

7   C. Graf, D. L. J. Vossen, A. Imhof and A. Van Blaaderen, *Langmuir*, 2003, **19**, 6693–6700.

8   A. K. Samal, L. Polavarapu, S. Rodal-Cedeira, L. M. Liz-Marzán, J. Pérez-Juste and I. Pastoriza-Santos, *Langmuir*, 2013, **29**, 15076–15082.

9   M. Grzelczak, J. Pérez-Juste, P. Mulvaney and L. M. Liz-Marzán, *Chem. Soc. Rev.*, 2008, **37**, 1783.

10   J. K. Young, N. A. Lewinski, R. J. Langsner, L. C. Kennedy, A. Satyanarayan, V. Nammalvar, A. Y. Lin and R. A. Drezek, *Nanoscale Res. Lett.*, 2011, **6**, 428.

11   M. Wuithschick, B. Paul, R. Bienert, A. Sarfraz, U. Vainio, M. Sztucki, R. Kraehnert, P. Strasser, K. Rademann, F. Emmerling and J. Polte, *Chem. Mater.*, 2013, **25**, 4679–4689.

12   Y. Sun and Y. Xia, *Science*, 2002, **298**, 2176–9.

13   A. Hu, P. Peng, H. Alarifi, X. Y. Zhang, J. Y. Guo, Y. Zhou and W. W. Duley, *J. Laser Appl.*, 2012, **24**, 042001.

14   T. Zhang, X.-Y. Zhang, X.-J. Xue, X.-F. Wu, C. Li and A. Hu, *Open Surf. Sci. J.*, 2011, **3**, 76–81.

15   S.-H. Cha, Y. Park, J. W. Han, K. Kim, H.-S. Kim, H.-L. Jang and S. Cho, *Sci. Rep.*, 2016, **6**, 32951.

16   A. Hu, J. Y. Guo, H. Alarifi, G. Patane, Y. Zhou, G. Compagnini and C. X. Xu, *Appl. Phys. Lett.*, , DOI:10.1063/1.3502604.

17   S. J. Kim and D. J. Jang, *Appl. Phys. Lett.*, 2005, **86**, 1–3.

18   J. A. Spechler and C. B. Arnold, *Appl Phys A*, 2012, **108**, 25–28.

19   S. Dai, Q. Li, G. Liu, H. Yang, Y. Yang, D. Zhao, W. Wang and M. Qiu, *Appl. Phys. Lett.*, , DOI:10.1063/1.4944699.

20   N. J. Borys, E. Shafran and J. M. Lupton, *Sci. Rep.*, 2013, **3**, 2090.

21   H. Huang, L. Liu, P. Peng, A. Hu, W. W. Duley and Y. Zhou, *J. Appl. Phys.*, , DOI:10.1063/1.4770476.

22   Z. Aabdin, J. Lu, X. Zhu, U. Anand, N. D. Loh, H. Su and U. Mirsaidov, *Nano Lett.*, 2014, **14**, 6639–6643.

23   Y. Q. Wang, W. S. Liang and C. Y. Geng, *Nanoscale Res. Lett.*, 2009, **4**, 684–688.

24   Z. Peng, B. Spliethoff, B. Tesche, T. Walther and K. Kleinermanns, *J. Phys. Chem. B*, 2006, **110**, 2549–2554.

25   E. C. Dreaden, A. M. Alkilany, X. Huang, C. J. Murphy and M. A. El-Sayed, *Chem. Soc. Rev.*, 2012, **41**, 2740–2779.

26   M. Vinod and K. G. Gopchandran, *Spectrochim. Acta - Part A Mol. Biomol. Spectrosc.*, 2015, **149**, 913–919.

27   V. A. Lobastov, R. Srinivasan and A. H. Zewail, *Proc. Natl. Acad. Sci. U. S. A.*, 2005, **102**, 7069–73.

28   D. Shorokhov and A. H. Zewail, *J. Chem. Phys. J. Chem. Phys. J. Chem. Phys. J. Appl. Phys. J. Chem. Phys.*, 2016, **144**, 80901–124706.

29   M. S. Grinolds, V. A. Lobastov, J. Weissenrieder and A. H. Zewail, *Proc. Natl. Acad. Sci.*, 2006, **103**, 18427–18431.

30   B. Barwick, H. S. Park, O.-H. Kwon, J. S. Baskin and A. H. Zewail, *Science (80-.).*, 2008, **322**, 1227–1231.

31   X. Xu, S. Kundu, T. Isik and V. Ortalan, *Microsc. Microanal.*, 2018, **24**, 1662–1663.

32   A. F. Oskooi, D. Roundy, M. Ibanescu, P. Bermel, J. D. Joannopoulos and S. G. Johnson, *Comput. Phys. Commun.*, 2010, **181**, 687–702.

33   H. J. Yang, S. Y. He and H. Y. Tuan, *Langmuir*, 2014, **30**, 602–610.

34   T. Liu, P. Jiang, Q. You and S. Ye, *CrystEngComm*, 2013, **15**, 2350–2353.

35   H. Yang, Y. Wang, X. Chen, X. Zhao, L. Gu, H. Huang, J. Yan, C. Xu, G. Li, J. Wu, A. J. Edwards, B. Dittrich, Z. Tang, D. Wang, L. Lehtovaara, H. Häkkinen and N. Zheng, *Nat. Commun.*, 2016, **7**, 12809.

36   P. Song and D. Wen, *J. Nanosci. Nanotechnol.*, 2010, **10**, 8010–8017.

37   A. Hu, P. Peng, H. Alarifi, X. Y. Zhang, J. Y. Guo, Y. Zhou and W. W. Duley, *J. Laser Appl.*, 2012, **24**, 042001.

38   F. Chen, S. Yang, Z. Wu, W. Hu, J. Hu and X. Duan, *Sci. China Mater.*, 2017, **60**, 39–48.

39   P. D. Nellist, in *Scanning Transmission Electron Microscopy*, 2011, pp. 91–115.

40   A. V. Crewe, J. Wall and J. Lanomore, *Science (80-.).*, , DOI:10.1126/science.168.3937.1338.

41   M. M. J. Treacy, A. Howie and C. J. Wilson, *Philos. Mag. A Phys. Condens. Matter, Struct. Defects Mech. Prop.*, , DOI:10.1080/01418617808239255.

42   S.-Y. Ding, J. Yi, J.-F. Li, B. Ren, D.-Y. Wu, R. Panneerselvam and Z.-Q. Tian, *Nat. Rev. Mater.*, 2016, **1**, 16021.

43   M. José-Yacamán, C. Gutierrez-Wing, M. Miki, D. Q. Yang, K. N. Piyakis and E. Sacher, *J. Phys. Chem. B*, 2005, **109**, 9703–9711.

44   K. E. J. Lehtinen and M. R. Zachariah, *Phys. Rev. B*, 2001, **63**, 205402.

45   K. E. J. Lehtinen and M. R. Zachariah, *J. Aerosol Sci.*, 2002, **33**, 357–368.

46   S. Link, Z. L. Wang and M. A. El-Sayed, , DOI:10.1021/jp990387w.

47   L. Rivas, S. Sanchez-Cortes, J. V. García-Ramos and G. Morcillo, *Langmuir*, 2000, **16**, 9722–9728.

48   I. Srnová-Šloufová, F. Lednický, A. A. Gemperle, J. Gemperlová, I. Srnova-Sloufova, F. Lednicky and J. Gemperlova, *Langmuir*, 2000, **16**, 9928–9935.

49   E. Csapó, A. Oszkó, E. Varga, Á. Juhász, N. Buzás, L. Korösi, A. Majzik and I. Dékány, *Colloids Surfaces A Physicochem.*

Eng. Asp., 2012, **415**, 281–287.

50   J. H. Hodak, A. Henglein, M. Giersig and G. V. Hartland*, , DOI:10.1021/JP002438R.

51   E. C. Garnett, W. Cai, J. J. Cha, F. Mahmood, S. T. Connor, M. Greyson Christoforo, Y. Cui, M. D. McGehee, M. L. Brongersma, M. G. Christoforo, Y. Cui, M. D. McGehee and M. L. Brongersma, *Nat. Mater.*, 2012, **11**, 241–9.

52   F. R. De Boer, R. Boom, W. C. M. Mattens, A. R. Miedema and A. K. Niessen, *Cohesion in Metals*, 1988, vol. 1.

53   H. L. Skriver and N. M. Rosengaard, *Phys. Rev. B*, 1992, **46**, 7157–7168.

54   M. Grouchko, P. Roitman, X. Zhu, I. Popov, A. Kamyshny, H. Su and S. Magdassi, *Nat. Commun.*, , DOI:10.1038/ncomms3994.

55   M. B. Mohamed, Z. L. Wang and M. a El-Sayed, *J. Phys. Chem. A*, 1999, **103**, 10255–10259.

56   Z. L. Wang, J. M. Petroski, T. C. Green and M. A. El-Sayed, *J. Phys. Chem. B*, 1998, **102**, 6145–6151.

57   J. H. Hodak, A. Henglein, M. Giersig and G. V. Hartland, *J. Phys. Chem. B*, 2000, **104**, 11708–11718.

58   † Tomohiro Shibata, *,† Bruce A. Bunker, ‡,§ Zhenyuan Zhang, *,‡,§ Dan Meisel, ‡,§ and Charles F. Vardeman II and ‡ J. Daniel Gezelter*, , DOI:10.1021/JA026764R.

59   D. B. Pedersen, S. Wang, E. J. Scott Duncan and S. H. Liang, *J. Phys. Chem. C*, 2007, **111**, 13665–13672.

60   P. Mulvaney, M. Giersig and A. Henglein, *J. Phys. Chem.*, 1993, **97**, 7061–7064.

61   Y. Cui, B. Ren, J. L. Yao, R. A. Gu and Z. Q. Tian, *J. Phys. Chem. B*, 2006, **110**, 4002–4006.

62   A. Kuzma, M. Weis, M. Daricek, J. Uhrik, F. Horinek, M. Donoval, F. Uherek and D. Donoval, *J. Appl. Phys.*, , DOI:10.1063/1.4864428.

63   I. Romero, J. Aizpurua, G. W. Bryant and F. J. García De Abajo, *Opt. Express*, 2006, **14**, 9988.

64   J. B. Lassiter, J. Aizpurua, L. I. Hernandez, D. W. Brandl, I. Romero, S. Lal, J. H. Hafner, P. Nordlander and N. R. Hales, *Nano Lett.*, 2008, **8**, 1212–1218.

65   O. Peña-Rodríguez, M. Caro, A. Rivera, J. Olivares, J. M. Perlado and A. Caro, *Opt. Mater. Express*, 2014, **4**, 403.

The structural and compositional evolution of Ag-Au nanoparticle dimers under laser irradiation were investigated using advanced electron microscopy techniques.